Study of ferroelectric characteristics of diisopropylammonium bromide films

C. Thirmal, P. P. Biswas, Y. J. Shin, T. W. Noh, N. V. Giridharan, A. Venimadhav, and P. Murugavel'

Study of ferroelectric characteristics of diisopropylammonium bromide films

C. Thirmal,[1] P. P. Biswas,[1] Y. J. Shin,[2,3] T. W. Noh,[2,3] N. V. Giridharan,[4] A. Venimadhav,[5] and P. Murugavel[1,a)]

[1]*Department of Physics, Indian Institute of Technology Madras, Chennai 600036, India*
[2]*Center for Correlated Electron Systems, Institute for Basic Science (IBS), Seoul 151-742, South Korea*
[3]*Department of Physics and Astronomy, Seoul National University (SNU), Seoul 151-742, South Korea*
[4]*Department of Physics, National Institute of Technology (NIT), Tiruchirappalli 620015, India*
[5]*Cryogenic Engineering Centre, Indian Institute of Technology Kharagpur, Kharagpur 721302, India*

Organic molecular ferroelectrics are highly desirable due to their numerous advantages. In the present work, a thick film of diisopropylammonium bromide organic molecular ferroelectric is fabricated on the ITO/glass substrate. The grown film shows preferential orientation along the *c*-axis with a ferroelectric transition at 419 K. The piezoresponse force microscopic measurements are done in a dual ac resonance tracking mode for its switching characteristics. The amplitude and phase images of the oppositely written domain patterns exhibit a clear contrast with 180° phase difference. The dynamical spectroscopic studies reveal a butterfly loop in amplitude and hysteretic character of the phase which are the expected characteristics features of ferroelectrics. In addition, the macroscopic polarization versus electric field hysteresis gives an additional proof for ferroelectric character of the film with the maximum polarization of 3.5 μC/cm^2. Overall, we have successfully fabricated diisopropylammonium bromide organic films and demonstrated its room temperature ferroelectric characteristics. *Published by AIP Publishing.*
[http://dx.doi.org/10.1063/1.4963754]

I. INTRODUCTION

Ferroelectrics are important multifunctional electroactive materials with versatile application potential in capacitors, actuators, non-volatile memory, and energy harvesting devices.[1–3] So far, oxides such as BaTiO$_3$, Pb(Zr,Ti)O$_3$, Bi$_{4-x}$La$_x$Ti$_3$O$_{12}$, etc., dominated the ferroelectric field due to their large polarization and piezoelectric coefficients.[4–6] However, high processing temperature and toxic heavy metal ions restrict their applications in microelectronic devices and even pose serious environmental problem.[7] As an alternative, the search on organic ferroelectrics has increased manifold. Astonishingly, the organic ferroelectrics have advantages such as eco-friendly, lightweight, cost-effective, scalable, and low processing temperature over their oxide counterparts.[8–10] The spontaneous polarization in organic ferroelectric originates either from cooperative migration of proton or from ordering of organic cation.[11–13] Although the ferroelectricity is discovered in numerous molecular organic compounds such as PVDF, nylon, imidazolium perchlorate, dabco perchlorate, 4-(cyanomethyl) anilinium perchlorate, and diisopropylammonium chloride,[8,14–16] most of them suffer from either low polarization or low thermal stability.[17] The recent discovery of ferroelectricity in diisopropylammonium bromide C$_6$H$_{16}$NBr (DIPAB) organic single crystal by Fu *et al.* renewed interest on this compound because of its large polarization (23 μC/cm^2) and good thermal stability (from 426 K down to liquid nitrogen temperature).[18] Among the organic ferroelectrics, the DIPAB will attract the scientific community due to its superior ferroelectric properties such as large polarization, good thermal stability, and high crystallinity. These unique features of

DIPAB pave the way to develop the ferroelectric based multi-functional materials such as magnetoelectric composites.[19] The single crystalline DIPAB shows centrosymmetric orthorhombic phase (P2$_1$2$_1$2$_1$) at room temperature, and it undergoes an irreversible phase transition to a non-centrosymmetric (polar) monoclinic phase (P2$_1$ space group) at 420 K. Subsequently, it exhibits a reversible paraelectric monoclinic (P2$_1$/m) phase transition at 426 K. The observed spontaneous polarization is attributed to the ordering of diisopropylammonium cation along *b*-axis, and the corresponding domain dynamics are studied on domains oriented along *b*-axis.[20,21] The large polarization of DIPAB comparable to BaTiO$_3$ and its good thermal stability along with the advantages of being an organic ferroelectrics makes it an excellent and intriguing compound for fundamental and technological studies.

However, the studies on this important compound are very limited, and as of our understanding, there are no reports on the DIPAB film. Looking at the break-through made by the ferroelectric oxide films, it is imperative to investigate the DIPAB film for better understanding and for its future realization in device applications. In the present work, though it is a challenging task to fabricate organic thin films, we have successfully fabricated DIPAB thick films on the ITO/glass substrates by the spin coating technique and explored its structural, dielectric, and ferroelectric properties. The switching characteristics of the fabricated *c*-axis oriented DIPAB film confirming its ferroelectric characteristics are reported in the present work.

II. EXPERIMENTAL DETAILS

To fabricate the film by spin-coating technique, optimized solution containing equi-molar quantity of diisopropylamine

a)Electronic mail: muruga@iitm.ac.in

and hydrobromic acid in methanol is used as a precursor. The adhesion and uniformity of the precursors on the substrate depend on the precursor concentration and the rpm during deposition. To optimize the growth condition, initially, the concentration of the solution is varied from 0.1 M to 7 M. At each concentration, 100 μl of the solution is spin coated on the cleaned ITO/glass at various rpm ranging from 1000 to 10 000. The pore free and continuous film is obtained at the 5 M concentrated solution which is spin coated at 2000 rpm. The obtained film is allowed to cure at 300 K for 24 h. Furthermore, the film is heat treated at 428 K for 10 min to get the desired ferroelectric monoclinic phase.[18] The fabricated films are subjected to X-ray diffraction (XRD) analysis using PANANALYTICAL X'Pert Pro X-ray diffractometer. The surface morphology of the film is obtained from Quanta 200 FEG scanning electron microscope (SEM). The dielectric studies are performed using NumetriQ (PSM1375) phase sensitive multimeter on the film in capacitor geometry with 1 mm diameter silver top electrode. The Oxford Instrument Asylum Cypher Piezoresponse Force Microscope (PFM) is employed to analyze the topography and local polarization switching. For the polarization versus electric field hysteresis loop measurements, gold is coated on the film by thermal evaporation by employing a shadow mask of each dot size 200 μm. Then, the hysteresis loop is measured using precision material analyzer (Radiant technologies).

III. RESULTS AND DISCUSSION

The XRD pattern for the heat treated DIPAB film is shown in Fig. 1(a) for 2θ ranging from 10° to 40°. For comparison, the XRD pattern for bulk DIPAB powder synthesized with the ferroelectric monoclinic phase by slow evaporation method[18,22] is shown in Fig. 1(b). Interestingly, Fig. 1(a) reveals diffraction peaks corresponding to (001), (002), and (003) reflections, and it indicates that the film is oriented along the c-axis with good crystalline quality. The corresponding d-spacing for planes (001), (002), and (003)

are 7.104, 3.549, and 2.365 Å, respectively. The observed diffraction peaks are consistent with the polar monoclinic phase of DIPAB. The surface morphology of the DIPAB film is studied by SEM, and the corresponding image is shown in Fig. 1(c). The image shows the surface is free from visible porosity which is essential for electrical characterization. It also shows that the surface has textured like morphology indicating possible preferred orientation of the film during growth on the ITO/glass substrate. The cross-sectional SEM image taken on the DIPAB film is shown as an inset in Fig. 1(c). From the cross-sectional SEM image, it is inferred that the film is grown with 18 μm thickness. To measure the average roughness of the grown film, PFM topographic imaging is done on the sample, and the resultant image is shown in Fig. 1(d). Fig. 1(d) reveals small grain like morphology at microscopic level. The measured average roughness of the film is around 4 nm.

In order to observe various phase transitions of the DIPAB film, dielectric measurements are carried out on the thick film. The film used for the measurement is cured at room temperature (300 K) after the spin coating (orthorhombic phase). The real and imaginary parts of dielectric constant (ε_r' and ε_r'') are plotted as a function of temperature from 380 to 430 K at various frequencies in Figs. 2(a) and 2(b), respectively. The ε_r' shows two transitions, namely, T_1 and T_2 at 413 and 419 K, respectively. The observed transitions in the DIPAB film are around 6 K lesser than reported single crystal values.[18,20] The decrease in the transition values cannot be attributed to strain effects in the film as it is a thick film. Though the exact reason is not clear to us, it could be due to defects formation during the film fabrication which is prominent in organic films. The transition at T_1 is attributed to the irreversible phase transition from orthorhombic ($P2_12_12_1$) to ferroelectric monoclinic ($P2_1$) phase. On the other hand, the transition at T_2 is attributed to reversible ferroelectric to paraelectric monoclinic ($P2_1/m$) phase. The frequency independent
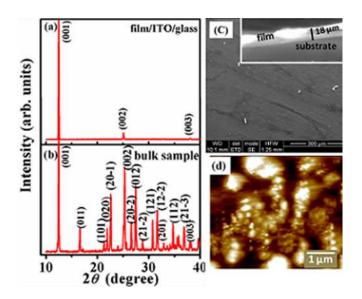

FIG. 1. X-ray diffraction pattern of DIPAB (a) film on the ITO/glass substrate and (b) bulk sample. (c) The SEM image of the DIPAB film surface and (d) PFM topographic image of the DIPAB film.
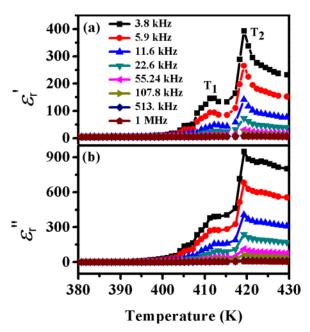

FIG. 2. Temperature variation of (a) ε_r' and (b) ε_r'' for the DIPAB film (cured at 300 K-orthorhombic-$P2_12_12_1$) at various frequencies.

sharp transition at T_2 indicates macroscopic evidence for ferroelectric nature of the sample. Similar measurements are carried out on the film which is subjected to heat treatment at 428 K (monoclinic phase). The corresponding ε_r' and ε_r'' as a function of temperature are plotted in Figs. 3(a) and 3(b) at various frequencies. Fig. 3 reveals a single transition at T_2. The absence of T_1 in heat treated film confirms its irreversible nature of the phase transition. These transitions are comparable with the single crystal data.[18,20]

The necessity of developing new ferroelectric materials for device applications requires understanding of their electromechanical and ferroelectric switching at nanometer scale. The PFM is a versatile tool for establishing the visualization of ferroelectric domains and their manipulation with applied voltage.[23] To understand ferroelectricity in the DIPAB film, ferroelectric domain switching measurements are performed on the heat treated sample using a vertical lithographic PFM in dual ac resonance tracking (DART) mode. The out-of-plane PFM measurement is done in the DART mode on the DIPAB film before writing, and the corresponding domain pattern is shown in Fig. 4. Fig. 4(a) represents the amplitude image, and Fig. 4(b) represents the phase image. The phase image shows the domain pattern where most of the domains are oriented at an average angle of 100° with respect to surface normal, indicating the in-plane orientation of domains. The corresponding line profiles for amplitude and phase are shown in Figs. 4(c) and 4(d), respectively. Since XRD reveals the *c*-axis oriented film, it is possible that the domains are aligned along in-plane polar *b*-axis.

To elucidate the ferroelectricity in the DIPAB film, in a selected $5 \times 5\ \mu m^2$ area, the domain pattern is written with $-10\ V$ at the central $3 \times 3\ \mu m^2$ area and with $+10\ V$ at the remaining area. The corresponding amplitude and phases are read simultaneously in the DART mode with an ac signal of 1.5 V. The resultant amplitude and phase images are shown in Figs. 5(a) and 5(b), respectively. The amplitude exhibits a
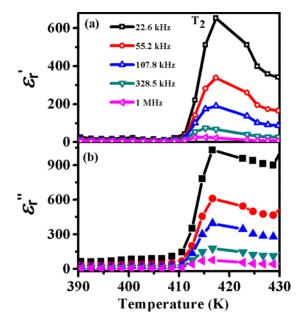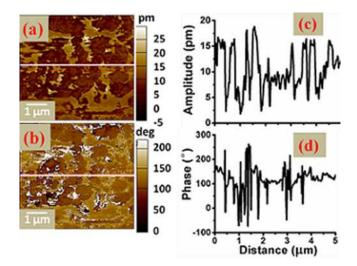

FIG. 4. The PFM (a) amplitude and (b) phase images of the DIPAB film (before writing). The corresponding line profiles are shown in (c) and (d).

clear contrast among oppositely written domain patterns. For clarity, the corresponding line profile is plotted in Fig. 5(c). The phase image in Fig. 5(b) exhibits a similar contrast with 180° phase difference among the written domain patterns (see the line profile plotted in Fig. 5(d)). The observed 180° phase difference gives a direct evidence for switchable domains in the DIPAB film and hence confirms its ferroelectric characteristics.

In DIPAB, the polarization direction is along the *b*-direction, i.e., along the in-plane direction of the film. However, the observed out-of-plane switching can be understood as follows. The piezoelectric tensor d_{ij} for C_2 point group of monoclinic system ($P2_1$) is given by

$$d_{ij} = \begin{pmatrix} 0 & d_{21} & 0 \\ 0 & d_{22} & 0 \\ 0 & d_{23} & 0 \\ d_{14} & 0 & d_{34} \\ 0 & d_{25} & 0 \\ d_{16} & 0 & d_{36} \end{pmatrix}.$$

FIG. 3. Temperature variation of of (a) ε_r' and (b) ε_r'' for the DIPAB film (heat treated at 428 K-monoclinic-$P2_1$) at various frequencies.
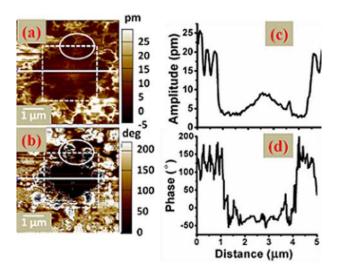

FIG. 5. The PFM (a) amplitude and (b) phase images of the DIPAB film (after writing). The corresponding line profiles are shown in (c) and (d).

By applying electric field along the *c*-axis, the corresponding converse piezoelectric effect is defined as $\varepsilon_j = d_{ij}E_i$, where $i = 1, 2, 3$ and $j = 1, 2, 3, 4, 5, 6$

$$\Rightarrow \begin{pmatrix} \varepsilon_1 \\ \varepsilon_2 \\ \varepsilon_3 \\ \varepsilon_4 \\ \varepsilon_5 \\ \varepsilon_6 \end{pmatrix} = \begin{pmatrix} 0 & d_{21} & 0 \\ 0 & d_{22} & 0 \\ 0 & d_{23} & 0 \\ d_{14} & 0 & d_{34} \\ 0 & d_{25} & 0 \\ d_{16} & 0 & d_{36} \end{pmatrix} \begin{pmatrix} 0 \\ 0 \\ E_3 \end{pmatrix}$$

$$\Rightarrow \varepsilon_4 = d_{34}E_3 \text{ and } \varepsilon_6 = d_{36}E_3,$$

i.e., ε_4 and ε_6 are non-zero components of shear strain about *a* and *c*-axes, respectively, under the application of electric field along the *c*-axis. Hence, the nonzero d_{36} component of piezoelectric tensor, for C_2 point group of monoclinic system, induces a shear strain under the influence of an electric field applied along *c*-axis.[24] This shear strain gives the vertical PFM switching response in the *c*-axis oriented DIPAB film. The PFM images shown in Fig. 5 exhibit a non-uniform switching behavior at regions near domain boundaries (marked as circle in Fig. 5(b)). Though the exact reason is not clear, this may be due to domain pinning or correlation effect as reported in oxide films.[25,26]

To further verify the polarization switching phenomenon in the DIPAB film, piezoresponse force spectroscopy is carried out in the DART mode where the out-of-plane piezoresponse is measured as a function of voltage. The obtained amplitude and phase response as a function of voltage are shown in Figs. 6(a) and 6(b), respectively. The amplitude plot reveals a clear butterfly loop reminiscent of ferroelectric character with two symmetrical minima at coercive fields. The phase graph shown in Fig. 6(b) reveals a hysteretic character with phase difference of 180° which is consistent with the phase profile shown in Fig. 5(b). The observed phase and amplitude behavior prove the polarization switching characteristics of the fabricated DIPAB film.

Apart from the microscopic proof of switching characteristics, for macroscopic switching characteristics, polarization versus electric field is measured at 300 K. The corresponding hysteresis loop is shown in Fig. 7. Fig. 7 exhibits a typical ferroelectric hysteresis loop of the DIPAB film. The asymmetric nature of loop may be attributed to the effect of dissimilar electrode configuration. Note that gold and ITO are used as top and bottom electrodes, respectively. The maximum polarization measured for the *c*-axis oriented DIPAB film is 3.5 μC/cm^2.

The field induced rotation of polarization in the monoclinic (bulk lattice parameters $a = 7.8689$, $b = 8.0976$, $c = 7.9093$ Å) DIPAB may be responsible for observed polarization along the non-polar axis in the presence of electric field. This type of field induced rotation was observed in various ferroelectrics BaTiO$_3$ and PbTiO$_3$ based systems. Note that the field induced polarization is more prominent in monoclinic systems.[27,28] Apart from field induced rotation, the 100° oriented domains in as grown sample observed in PFM (Fig. 4) may also add their component to the observed *c*-axis polarization in the presence of electric field. The maximum polarization observed along the *c*-axis is 3.5 μC/cm^2, and it is smaller than the reported polarization along the *b*-axis. However, it is still larger than the values reported for other organic ferroelectrics in literature. Hence, the observed polarization value along the *c*-axis may be partly due to field induced rotation and partly due to the b-axis polarization component originated at the expense of decrease in polarization along the *b*-axis. A schematic representation of the polarization direction in single crystal and film (in the presence and absence of electric field) is shown in Fig. 8. Ironically, the P-E measurements carried out on the DIPAB single crystal were all done just below (1 or 2 K) the ferroelectric Currie temperature (<428 K) and not at room temperature for reasons not known.[18,20] Thus, P-E hysteresis loop measured at 300 K gives the macroscopic evidence for ferroelectricity in the *c*-axis oriented DIPAB films without any ambiguity. However, the study of DIPAB with its polar *b* axis being in the out-of-plane direction would be important and interesting for its future applications. The advantage of
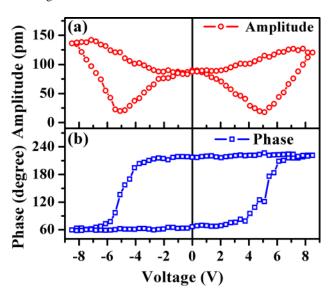
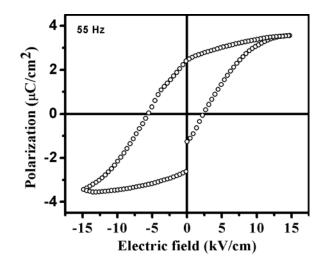FIG. 6. The piezoresponse spectroscopic (a) amplitude and (b) phase response of the DIPAB film.

FIG. 7. The polarization versus electric field measured at 300 K for DIPAB film.
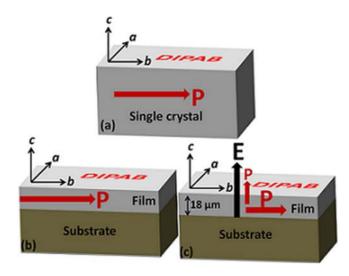
FIG. 8. A schematic representation of polarization direction in DIPAB: (a) single crystal, (b) *c*-axis oriented thick film in the absence of electric field, and (c) *c*-axis oriented thick film in the presence of electric field.

DIPAB films is that they can be coated on the flexible substrates and hence used for dielectric based flexible capacitor applications apart from sensors and memory devices.

IV. CONCLUSIONS

In conclusion, the *c*-axis oriented DIPAB film is grown on the ITO/glass substrate by the spin coating technique. The X-ray diffraction confirmed the *c*-axis orientation of the film with good crystalline quality. The frequency independent transition observed in temperature variation of dielectric constant indicated the ferroelectric transition in the film. The phase and amplitude image of the domain pattern written by lithographic PFM proved local domain switching behavior. The PFM spectroscopic analysis was carried out as a function of voltage showed the butterfly loop for amplitude and hysteresis loop with a clear 180° phase difference for phase confirming the ferroelectric characteristics of the film. Finally, the macroscopic evidence for room temperature ferroelectric switching is revealed by polarization versus electric field hysteresis measurements. Though the films are 18 μm thick, information obtained about the ferroelectric characteristics of *c*-axis oriented thick film can also be extended to thin film of the same orientation. Environmentally friendly, transparent, light weight, and scalable organic ferroelectric are in need of today's electronic industry, and in the present work, we partly succeeded in achieving the same in the DIPAB film.

[1]S. Horiuchi and Y. Tokura, Nat. Mater. **7**, 357 (2008).
[2]A. Gruverman, B. J. Rodriguez, C. Dehoff, J. D. Waldrep, A. I. Kingon, R. J. Nemanich, and J. S. Cross, Appl. Phys. Lett. **87**, 082902 (2005).
[3]R. Xu, S. Liu, I. Grinberg, J. Karthik, A. R. Damodaran, A. M. Rappe, and L. W. Martin, Nat. Mater. **14**, 79 (2015).
[4]O. Trithaveesak, J. Schubert, and Ch. Bucha, J. Appl. Phys. **98**, 114101 (2005).
[5]B. S. Kang, D. J. Kim, J. Y. Jo, T. W. Noh, J. G. Yoon, T. K. Song, Y. K. Lee, J. K. Lee, S. Shin, and Y. S. Park, Appl. Phys. Lett. **84**, 3127 (2004).
[6]B. H. Park, B. S. Kang, S. D. Bu, T. W. Noh, J. Lee, and W. Jo, Nature **401**, 682 (1999).
[7]W. Gao, L. Chang, H. Ma, L. You, J. Yin, J. Liu, Z. Liu, J. Wang, and G. Yuan, NPG Asia Mater. **7**, 189 (2015).
[8]Y. Zhang, Y. Liu, H. Y. Ye, D. W. Fu, W. Gao, H. Ma, Z. Liu, Y. Liu, W. Zhang, J. Li, G. L. Yuan, and R. G. Xiong, Angew. Chem., Int. Ed. **53**, 5064 (2014).
[9]M. Caironi, D. Natali, M. Sampietro, C. Bertarelli, A. Bianco, A. Dundulachi, E. Canesi, and G. Zerbi, Appl. Phys. Lett. **89**, 243519 (2006).
[10]S. Chen and X. C. Zeng, J. Am. Chem. Soc. **136**, 6428 (2014).
[11]A. P. Bisiorek, A. Białonska, R. Jakubas, P. Zielinski, M. Wojciechowska, and M. Gatazka, Adv. Mater. **27**, 5023 (2015).
[12]A. S. Tayi, A. Kaeser, M. Matsumoto, T. Aida, and S. I. Stupp, Nat. Chem. **7**, 281 (2015).
[13]J. Li, Y. Liu, Y. Zhang, H. L. Cai, and R. G. Xiong, Phys. Chem. Chem. Phys. **15**, 20786 (2013).
[14]A. Katrusiak and M. Szafranski, Phys. Rev. Lett. **82**, 576 (1999).
[15]H. L. Cai, W. Zhang, J. Z. Ge, Y. Zhang, K. Awaga, T. Nakamura, and R. G. Xiong, Phys. Rev. Lett. **107**, 147601 (2011).
[16]D. W. Fu, W. Zhang, H. L. Cai, J. Z. Ge, Y. Zhang, and R. G. Xiong, Adv. Mater. **23**, 5658 (2011).
[17]J. Zhu, K. Gao, S. Xiao, X. Qiu, H. L. Cai, and X. S. Wu, Phys. Chem. Chem. Phys. **17**, 4029 (2015).
[18]D. W. Fu, H. L. Cai, Y. Liu, Q. Ye, W. Zhang, Y. Zhang, X. Y. Chen, G. Giovannetti, M. Capone, J. Li, and R. G. Xiong, Science **339**, 425 (2013).
[19]J. X. Zhang, J. Y. Dai, L. C. So, C. L. Sun, C. Y. Lo, S. W. Or, and H. L. W. Chan, J. Appl. Phys. **105**, 054102 (2009).
[20]A. Piecha, A. Gagor, R. Jakubas, and P. Szklarz, CrystEngComm **15**, 940 (2013).
[21]H. Lu, T. Li, S. Poddar, O. Goit, A. Lipatov, A. Sinitskii, S. Ducharme, and A. Gruverman, Adv. Mater. **27**, 7832 (2015).
[22]C. Thirmal, P. Murugavel, and V. Subramanian, Curr. Appl. Phys. **14**, 688 (2014).
[23]S. V. Kalinin, A. N. Morozovska, L. Q. Chen, and B. J. Rodriguez, Rep. Prog. Phys. **73**, 056502 (2010).
[24]J. F. Nye, *Physical Properties of Crystals* (Oxford University Press, New York, 1957).
[25]W. J. Hu, D. M. Juo, L. You, J. Wang, Y. C. Chen, Y. H. Chu, and T. Wu, Sci. Rep. **4**, 4772 (2014).
[26]Y. Ivry, J. F. Scott, E. K. H. Salje, and C. Durkan, Phys. Rev. B **86**, 205428 (2012).
[27]M. Davis, M. Budimir, D. Damjanovic, and N. Setter, J. Appl. Phys. **101**, 054112 (2007).
[28]H. Fu and R. E. Cohen, Nature **403**, 281 (2000).